GA–A27477

THE GENERAL ATOMICS FUSION THEORY PROGRAM REPORT FOR GRANT YEAR 2012

by
PROJECT STAFF

NOVEMBER 2012

GENERAL ATOMICS

DISCLAIMER

GA–A27477

THE GENERAL ATOMICS FUSION THEORY PROGRAM REPORT FOR GRANT YEAR 2012

by
PROJECT STAFF

Work supported by
the U.S. Department of Energy
under Grant No. DE-FG02-95ER54309

GENERAL ATOMICS PROJECT 03726
NOVEMBER 2012

GENERAL ATOMICS

ABSTRACT

The objective of the fusion theory program at General Atomics (GA) is to significantly advance our scientific understanding of the physics of fusion plasmas and to support the DIII-D and other tokamak experiments as well as ITER research activities. The program plan is aimed at contributing significantly to the Fusion Energy Science, the Tokamak Concept Improvement, and ITER goals of the Office of Fusion Energy Sciences (OFES). Significant progress was made in each of the important areas of our research program during the last grant period GY12. This includes application of the EPED model to develop a new working model for RMP ELM suppression and tested it against DIII-D discharges; GYRO simulations of screened RMP induced turbulent island torque; successful comparison of M3DC1 modeling of the electron temperature profile displacements and magnetic structures in the DIII-D plasma edge upon the application of non-axisymmetric fields with experimental data; identification of two candidate physical processes that may be used to enhance the plasma resistivity for runaway electron mitigation in a gas-jet study; demonstration with NIMROD simulations of a DIII-D massive gas injection experiment that even a perfectly toroidally symmetric impurity source produces radiation asymmetry due to the role of the 1/1 MHD mode; formulation of a nonlinear theory of drift-cyclotron kinetics to investigate the breakdown of gyro-kinetics; demonstration that the flux prediction of GYRO local simulations is able to capture the more computationally intensive globally predicted energetic-particle and thermal-ion flux profiles; developed and tested a TGLF driven DEP code for passive radial and energy space diffusion of energetic particles; demonstration with TGLF modeling of a set of 26 H-mode discharges from the DIII-D stiffness experiments that the temperature profile shape varies weakly over a three-fold increase in neutral-beam power consistent with experimental observations; development and improvement of the new “spectral-shift” paradigm for $E\times B$ Doppler shear after extensive verification with GYRO results; demonstration with NEO comparison of collision models on neoclassical transport in the plasma edge that using the full linearized Fokker-Planck operator becomes more important further into the edge; demonstration with ORBIT-RF/AORSA simulations of DIII-D high-harmonic fast-wave (FW) experiments that the synergistic effect observed in the DIII-D two-frequency FW heating experiments is due to finite Larmor radius effects; and development of a new Python-based integrated modeling framework OMFIT that facilitates efficient interactions among modules by treating them as a collection of objects organized in a MDSPlus-like tree structure.

TABLE OF CONTENTS

1. HIGHLIGHTS OF THEORY WORK IN GY12

During the past grant year, significant progress was made in each of the important areas of our research program:

- Demonstration with MARS calculations that both the in-board and out-board plasma magnetic responses to 3D non-axisymmetric fields are significant and the out-board plasma response becomes stronger as beta increases as part of the DIII-D magnetic design study.
- Demonstration with M3DC1 and NIMROD calculations of magnetic helicity that it undergoes discrete jumps where islands form during the nonlinear evolution with additional change away from the island regions.
- Application of the EPED model to develop a new working model for RMP ELM suppression in which the penetrated perturbation field stops the inward propagation of the edge barrier before the peeling-ballooning mode becomes unstable when the resonant surfaces are in the proper location and tested it against DIII-D discharges.
- Demonstration with ELITE analysis of DIII-D discharges from a pellet-pacing experiment that the pellet-triggered ELMs are driven by local physics associated with the pellet deposition.
- Successful comparison of M3DC1 modeling of the electron temperature profile displacements and magnetic structures in the DIII-D plasma edge upon the application of non-axisymmetric fields with Thomson scattering and soft x-ray emission data.
- Successful calculations of single-fluid nonlinear 3D response to perturbation magnetic fields with M3DC1 using nearly realistic parameters for the first time that show a strong kink-like response.
- Identification of two candidate physical processes that may be used to enhance the plasma resistivity for runaway electron mitigation in a gas-jet study.
- Demonstration with NIMROD simulations of a DIII-D massive gas injection experiment that even a perfectly toroidally symmetric impurity source produces radiation asymmetry due to the role of the 1/1 MHD mode in convecting both heat from the core to edge and impurities from edge to core.
- Modification of GYRO and TGYRO to enable operation in hybrid mode that combines distributed-memory parallelization using MPI with shared-memory parallelization using OpenMP showing significant performance improvement.

- Demonstrated with GYRO simulations that minimum screening of RMP induced turbulent island torque is at the electron rest point (i.e. electron not ion radial force balance).
- Development of a reduced model for 6D cyclo-kinetics to test the breakdown of 5D gyro-kinetics by following dynamics in the gyro-phase.
- Initial development of a new gyro-kinetic code suitable for the highly collisional plasma edge pedestal region as a gyro-kinetic extension of NEO.
- Demonstration with GYRO simulations of Alfvén eigenmodes in DIII-D that the form of the driving energetic-particle distribution function plays an important role in accurately determining the real frequency and growth rate of energetic-particle driven Alfvén-sonic modes such as the beta induced Alfvén eigenmode (BAE).
- Developed and tested a TGLF driven DEP code for passive radial and energy space diffusion of energetic particles against GYRO simulations.
- Demonstration that the flux prediction of GYRO local simulations is able to capture the more computationally intensive globally predicted energetic-particle and thermal-ion flux profiles well with a saturation model.
- Demonstration with TGLF modeling of a set of 26 DIII-D H-mode discharges from the transport stiffness experiments that the temperature profile shape varies weakly over a 3-fold increase in neutral-beam power consistent with experimental observations.
- Demonstration with TGLF modeling of reversed-shear low and high beta DIII-D discharges that radially extending the location of the minimum safety factor increases the plasma stored energy and broadens the pressure profile.
- Development and improvement of the new “spectral-shift” paradigm for $E\times B$ Doppler shear after extensive verification with GYRO results.
- Initial development of a new 3D local analytic equilibrium solver analogous to a 3D extension of the Miller formalism for shaped axisymmetric equilibria for use with the neoclassical code NEO to explore the non-axisymmetric effects on transport.
- Demonstration with NEO comparison of collision models on neoclassical transport in the plasma edge that using the full linearized Fokker-Planck operator becomes more important further into the edge.
- Demonstration with ORBIT-RF/AORSA simulations of DIII-D high-harmonic fast-wave (FW) experiments that the synergistic effect observed in the DIII-D two-frequency FW heating experiments is due to coupling of the two harmonics by finite drift orbits.
- Development of a new general pellet ablation model based on a Fokker-Planck treatment of the electron heat-flux attenuation in the expanding ablation shield and its

application to predict the penetration depth and density profile in ITER after injection of a pellet.

- Development of a new Python-based integrated modeling framework OMFIT that facilitates efficient interactions among modules by treating files, data, and scripts as a collection of objects organized in a MDSPlus-like tree structure.

As a consequence of these results, scientists from the Theory Group were selected to give a number of invited talks and colloquia as highlighted in the next section. Sections 3–6 provide more detailed descriptions of the advances and achievements made in each of the major areas. A list of publications is given in Section 7.

2. SIGNIFICANT PRESENTATIONS IN GY12

2012 PRESENTATIONS

24TH IAEA Fusion Energy Conference in San Diego, USA October 8–13, 2012:

- E.M. Bass gave a presentation “Fully Gyro-Kinetic Modeling of Beam-Driven Alfvén Eigenmodes in DIII-D Using GYRO.”
- N.M. Ferraro gave a presentation “Edge Plasma Response to Non-Axisymmetric Fields in Tokamaks.”
- V.A. Izzo gave a presentation “Impurity Mixing in Massive-Gas-Injection Simulations of DIII-D.”
- P.B. Snyder gave an presentation “The EPED Pedestal Model: Extensions, Application to ELM-Suppressed Regimes, and ITER Predictions.”
- G.M. Staebler gave an oral presentation “A New paradigm for E×B Velocity Shear Suppression of Gyro-Kinetic Turbulence and the Momentum Pinch.”

54TH APS DPP meeting in Providence, Rhode Island October 29 – November 2, 2012:

- J. Candy gave an invited tutorial presentation “Theory, Verification and Validation of Finite-Beta Gyro-Kinetics.”
- V.A. Izzo gave an invited presentation “Impurity Mixing, Radiation Asymmetry, and Runaway Electron Confinement in MGI Simulations of DIII-D and ITER.”
- A.D. Turnbull gave an invited presentation “Comparisons of Linear and Nonlinear Plasma Response Models for Non-Axisymmetric Perturbations.”
- R.E. Waltz gave an invited presentation “Search for the Missing L-Mode Edge Transport and Possible Breakdown of Gyro-Kinetics.”

18TH International Stellarator Workshop in Canberra, Australia January 29 – February 3 2012:

- A.D. Turnbull gave a presentation “Comparison of Plasma Response Models for Non-axisymmetric Perturbations.”

USBPO Disruption Mitigation Workshop in San Diego, California March 12–13 2012:

- V. Izzo gave a presentation “Disruption Mitigation Modeling Work.”

APS-Sherwood Meeting in Atlanta, Georgia March 31 – April 3, 2012:

- Ron Waltz gave an invited presentation "Gyro-Kinetic Simulations with External Resonant Magnetic Perturbations: Island Torque and Non-Ambipolar Transport with Rotation."

ITPA Pedestal Topical Meeting Hefei, China April 2–4, 2012:

- P.B. Snyder gave a presentation "An EPED-Based Working Model for RMP ELM Suppression" and a summary presentation "Discussion of Progress and Work Plan for ITER Urgent Issues in Pedestal Structure."

US Transport Task Force Workshop in Annapolis, MD April 10–13, 2012:

- P.B. Snyder gave a presentation "Developing and Testing the EPED Model for the 2011 JRT on Pedestal Structure."

39TH EPS Conference on Plasmas Physics in Stockholm, Sweden July 2–6, 2012:

- M. Choi gave a presentation "Modeling of Large Orbit Fast Ion Distribution Evolution with Multiple Frequency FW Heating."

EFTSOMP Workshop in Stockholm, Sweden July 9–10, 2012:

- R.E. Waltz gave an invited talk on "Gyro-Kinetic Simulations with External Resonant Magnetic Perturbations: Island Torque and Non-Ambipolar Transport with Rotation."

6TH US-PRC Magnetic Fusion Collaboration Workshop in San Diego, California July 10–12, 2012:

- Orso Meneghini gave a presentation "OMFIT: A New Approach to Integrated Modeling."

Magnetic Fusion Theory and Simulation Workshop in Hefei, China July 16–17, 2012:

- L.L. Lao gave a presentation "Recent Progress in Theory and Modeling of DIII-D Experiments."

International School of Plasma Physics in Varenna, Italy August 27–31, 2012:

- N.M. Ferraro gave a presentation "Modeling Edge Plasma Response to Non-Axisymmetric Magnetic Fields in Tokamaks."

EU Transport Task Force Workshop in Padua, Italy September 3–6, 2012:

- G.M. Staebler gave an invited presentation "Transport in the Core-Edge Transition Region."

3. ADVANCES IN MHD EQUILIBRIUM AND STABILITY RESEARCH

3.1. 3D EQUILIBRIUM STUDY AND MAGNETIC HELICITY

DIII-D 3D Magnetic Diagnostic Study: A post-processor to simulate magnetic diagnostic signals and radial displacements due to 3D non-axisymmetric coils based on Fortran 90 and MARS output file RZDATA was constructed and applied to support DIII-D 3D magnetic diagnostic design. Analysis results indicate that the plasma contribution to the magnetic signals is small as expected and appropriate magnetic probe connections are necessary to enhance the probe signals for extraction of plasma response.

MARS analyses were also performed to support the magnetic diagnostic design study. The study included a β and a q scan. MARS results show that both the in-board and the out-board plasma responses are significant and the out-board plasma response becomes stronger as β increases.

Magnetic Helicity in 3D Equilibria Transformations: Work to understanding the role of helicity in equilibria undergoing transformations was continued. Magnetic helicity was calculated in the M3DC1 and NIMROD codes to test the hypothesis that the helicity should undergo discrete jumps where islands form during the nonlinear evolution, but remain unchanged in between except for an additive constant. While jumps do occur as expected, the results found that there is not simply an offset, as some additional change in helicity is evident away from island regions.

3.2. PEDESTAL MODEL DEVELOPMENT, VALIDATION, AND ANALYSIS

EPED Pedestal Model Analysis and Extension: The EPED pedestal model was used to develop a new working model for understanding suppression of ELMs via resonant magnetic perturbations (RMP). EPED combines calculated kinetic ballooning mode (KBM) and peeling-ballooning (P-B) constraints to predict the pedestal height and width. In ELMing plasmas, the KBM constrains the pressure gradient, but the pedestal width can continue to broaden until there is sufficient free energy to destabilize a P-B mode, which triggers the ELM. We hypothesize that in RMP ELM suppression, the applied RMP is able to penetrate near the top of the pedestal where the electron perpendicular velocity is small. If the resonant surfaces are in the proper location, this penetrated field perturbation can stop the inward propagation of the edge barrier before the P-B mode becomes unstable, suppressing the ELM, as shown in Fig 1. Calculating the required resonant surface locations for this process generates predicted ranges of safety factor (q) that are in good agreement with the observed q windows for ELM suppression. The prediction that pedestal width is reduced while gradients remain approximately constant is in agreement with observations on DIII-D using a recently upgraded high resolution Thomson system.

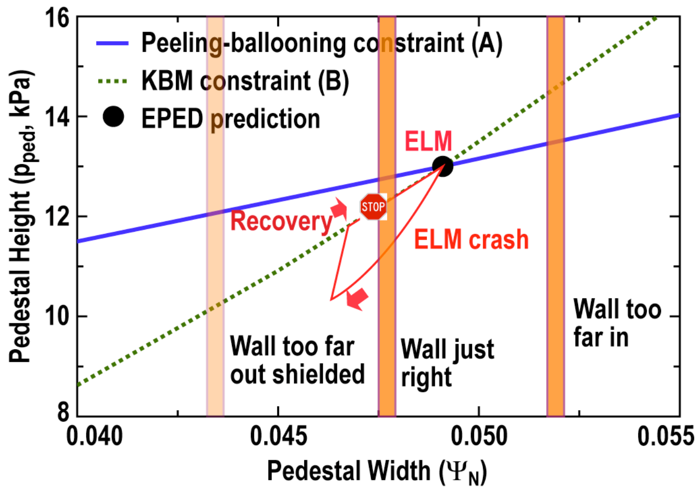

Fig. 1. Illustration of the working model for RMP ELM suppression based on the EPED pedestal model. The EPED model predicts the pedestal height and width based on the combination of calculated peeling-ballooning (solid line) and KBM (dashed line) constraints. The EPED predicted pedestal height and width (at which an ELM would occur) is shown by the black circle. A typical ELM cycle is shown in red. We hypothesize that the RMP field is able to penetrate near the top of the pedestal, potentially forming a "wall" that prevents further inward penetration of the edge barrier. If this "wall" is placed in just the right position (center location on the figure) it can block the recovery part of the ELM cycle, suppressing the ELM (denoted by octagonal "stop" sign on the figure). This correct location for suppressing the ELM corresponds to a predicted range of q values for ELM suppression, which in an initial test agrees with the observed q windows for ELM suppression.

The EPED-based working model for RMP ELM suppression was tested on a pair of DIII-D discharges. In the first discharge, the safety factor (q_{95}) is inside the resonant window, and ELMs are fully suppressed. In the second discharge, q_{95} is outside the resonant window and ELMs remain. The EPED model predicts a critical pedestal width of ~3%, above which the ELM is expected to be triggered. In the ELM-suppressed discharge, the pedestal width is constrained below this value (~1.9%) and hence no ELMs are expected, consistent with observations. In the discharge with ELMs, the pedestal width reaches the predicted critical width (~3%) just before the ELM is triggered. These results are consistent with the model, in which a "wall" provided by strong RMP transport associated with rational surfaces blocks the inward expansion of the pedestal, suppressing the ELM. Further tests of the working model for RMP-ELM suppression are ongoing.

Peeling-ballooning (P-B) stability studies with the ELITE code have been conducted on a series of plasmas in which ELMs were suppressed by increasingly strong resonant magnetic perturbations (RMPs) applied by the I-coil on DIII-D. In a scan of I-coil current, ELMs are observed for zero or 4 kA of I-coil current, ELMs are mostly suppressed at 4.8 kA, and completely suppressed at higher values. The P-B stability study finds that when ELMs occur, the plasma is at or near the P-B instability threshold, while for full suppression, the plasma is stable to P-B modes. This result is consistent with the P-B mode being the ELM trigger, and stabilization of the P-B mode being an essential aspect of RMP ELM suppression. This result is also consistent with the working model for RMP ELM suppression based on the EPED model.

The EPED pedestal model was also applied to Quiescent H-Mode (QH) discharges in which steady H-mode conditions are achieved without ELMs. EPED predictions for the pedestal height and width in 11 QH-mode discharges are found to agree well with observations (within ~20%, correlation coefficient ~0.9), including cases in which very high pedestals are achieved (Fig. 2). This agreement gives confidence in the ability of EPED to predict the critical density for QH-mode operation in ITER and other devices. EPED predicts that ITER will operate in the density range expected to allow QH-mode operation, but other requirements, such as that for rotation, remain under investigation.

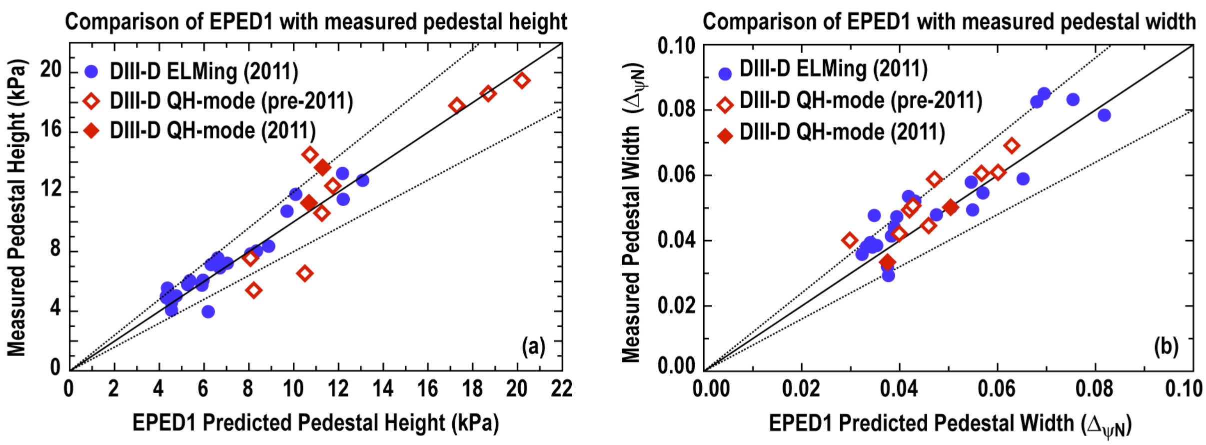

Fig. 2. Comparison of EPED predicted pedestal height (a) and width (b) for a set of quiescent mode discharges from 2011 (solid diamonds) and earlier years (open diamonds). Also shown for comparison are a set of 24 ELMing discharges from 2011.

A major upgrade to the Thomson scattering system on DIII-D allows higher resolution measurements of the pedestal, providing stringent tests of the EPED model for pedestal height and width. A series of DIII-D experiments was conducted in which the plasma current and magnetic field were varied, yielding factor of ~3 variation in the pedestal height and width. The EPED model was found to be in very good agreement with observations from high resolution measurements, with a ratio of predicted to observed pedestal height of 0.98 ± 0.15 (correlation of 0.96) and a ratio of predicted to observed pedestal width of 0.94 ± 0.13 (correlation of 0.91) in 24 cases.

ELITE Edge Stability Analysis: The ELITE code was used to study edge stability of a series of DIII-D discharges in which pellets are used to trigger edge localized modes (ELMs). Without pellets, the pedestal evolves towards a peeling-ballooning unstable state, at which large ELMs are triggered. However, with the pellets triggering rapid, small ELMs, ELITE finds that the pedestal remains in the stable region. This suggests that the pellet-triggered ELMs are driven by local physics associated with the pellet deposition. Notably, in the pellet driven case, the pedestal remains narrow, while without pellets, the pedestal broadens until the ELM occurs. This suggests that the pellets interrupt the natural ELM cycle at a time when the pedestal is too narrow for the natural ELM to occur.

ELITE was also used to study edge stability in ITER baseline discharges on DIII-D with strong electron heating, and suppress of ELMs by resonant magnetic perturbations (RMP). Without the RMP, the discharges become unstable to peeling-ballooning modes and ELMs occur. During RMP ELM suppression, the discharge remains in the stable region.

3.3. PLASMA RESPONSE TO EXTERNAL PERTURBATION FIELDS

Non-axisymmetric Plasma Response Modeling: As part of the FES Theory Milestone on Non-axisymmetric Fields in Tokamak Equilibria, comparisons among M3DC1, MARS-F, IPEC, and VMEC calculations of the plasma response were performed. As in DIII-D discharge 126006, calculations using MARS-F and VMEC of the response for DIII-D discharge 142603 with internal $n = 3$ coils confirmed that linear and nonlinear predictions yield qualitatively different results for the perturbed flux surfaces. The linear results from MARS-F, in contrast, are in reasonably good agreement with other linear predictions from IPEC and M3DC1. Investigation of reasons for the discrepancy with VMEC suggests that even though the applied fields are a small fraction of the axisymmetric field, finite linearized displacements can lead to flux surfaces crossing, invalidating the linear model. A sufficient criterion for crossing was derived in terms of when the initial and final points of the finite displacement differ in phase by more than $\pi/2$. For discharge 142603, a map of where this phase difference exceeds $\pi/2$ shows multiple regions occur, particularly on the inboard side where the discrepancy is most pronounced

One potential obstacle in these comparisons is that the VMEC calculation reports the perturbed surfaces, whereas linear calculations report the "displacements" of surfaces, which agree with the actual surface locations (as calculated by field line integration) only in the limit of small displacements. A method was developed for calculating and geometrically scaling the surfaces from field line integration of M3DC1, for a more accurate comparison with VMEC. This method showed that the "displacement" overestimates the surface perturbation on the high-field side and underestimates the perturbation on the low-field side, bringing results in closer agreement with VMEC. However, substantial differences with the VMEC results remain.

M3DC1 Development: New developments in M3DC1 allow more accurate calculations of non-axisymmetric plasma response, and closer comparison with experiment. First, several improvements in the meshing capability allow strongly anisotropic field-aligned adaptation, which allows for radial resolution on the order of a few millimeters (previously, radial resolution had been limited to 1–2 centimeters). Improvements to the internal Grad-Shafranov solver allow empirical electron temperatures to be specified, and the ion mass and effective Z of the plasma may now also be specified.

Recent M3DC1 development work sought to enable transport calculations using the 3D fields calculated with M3DC1. One such effort has been the development of a software library that allows TRIP3D to import magnetic field data from M3DC1 output. This capability has recently begun to be used to quantify the effects of plasma response on edge stochasticity. It is found that the effect of the plasma response is to significantly reduce the stochasticity of the edge relative to the level predicted by vacuum modeling, even in the case of incomplete screening, due to the highly nonlinear dependence of magnetic diffusivity on island size. This software library has also recently been adapted to provide vector potential data from M3DC1 in a form that can be used by the particle orbit tracing code, ORBIT-RF. This will allow the study of fast-ion loss due to non-axisymmetric fields in the presence of plasma response. Finally, both NEO and M3DC1 have been modified to support an ongoing ITER task for modeling the plasma response to non-axisymmetric coils in ITER. These modifications include the capability to convert CORSICA output files into GYRO input files, and the capability to read velocity data from NEO into M3DC1.

Two new tools for analyzing M3DC1 output were also developed. The first is an IDL post-processing routine for evaluating the Cole formulation of Neoclassical Toroidal Viscosity (NTV) from M3DC1 output. This allows the NTV from 3D fields to be calculated taking into account the resistive, two-fluid plasma response. This I/O library is being used by virtual diagnostics for forward modeling of soft x-ray emissions in the plasma edge. Second, a Python interface to the M3DC1 I/O library was developed and deployed on the GA cluster. This interface is being used to read and display M3DC1 data through the OMFIT framework.

M3DC1 Non-axisymmetric Plasma Response Modeling: Two-fluid modeling of 3D plasma response has been carried out for a number of DIII-D discharges for the purpose of comparing with experimental measurements. In particular, the measured displacement of the electron temperature profile upon the application of non-axisymmetric fields were found generally to agree well both in phase and magnitude with the results of M3DC1 modeling (Fig. 3). M3DC1 results also compare favorably with changes in the measured soft x-ray emission in the plasma edge when non-axisymmetric fields are applied. These measurements clearly show field-aligned helical structures resulting from the applied fields, as can be seen in (Fig. 4). These results contribute to our understanding of RMP ELM suppression, and were presented at the 2012 IAEA fusion energy conference.

Two-fluid calculations with M3D-C1 have also been carried out using experimental profiles from DIII-D discharge 126006 in order to investigate island formation near the top of the pedestal during RMP ELM suppression. Consistent with previous results, it is found that islands are largest near the point where electron rotation vanishes; in this case near ψ_N = 0.85. Still, incomplete screening is found as far out as ψ_N = 0.95, consistent with the hypothesis that islands may limit pedestal width in RMP ELM suppressed cases. More analysis is needed to understand the extent to which island penetration is correlated with ELM suppression.

M3D-C1 Non-Linear Plasma Response: Preliminary calculations of nonlinear 3D response were also undertaken with M3DC1. Single-fluid calculations using nearly realistic parameters (Spitzer resistivity, κ, μ ~ 100 m^2/s) have been successfully run for the first time. Initial results show a strong kink-like response; however, this may be a transient response that has not fully decayed in time.

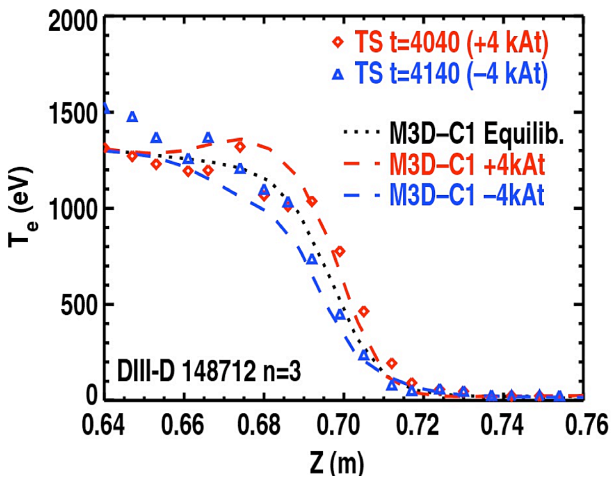

Fig. 3. Electron temperature measurements from Thomson scattering (symbols) for DIII-D discharge 148712 in the presence of 4 kA (red) and –4 kA (blue) current in the I-coils are compared to those modeled by M3DC1 (dashed lines). Here the I-coils are operated in even-parity n=3 configuration. The temperature profile of the axisymmetric equilibrium reconstruction is shown by the black dotted line.

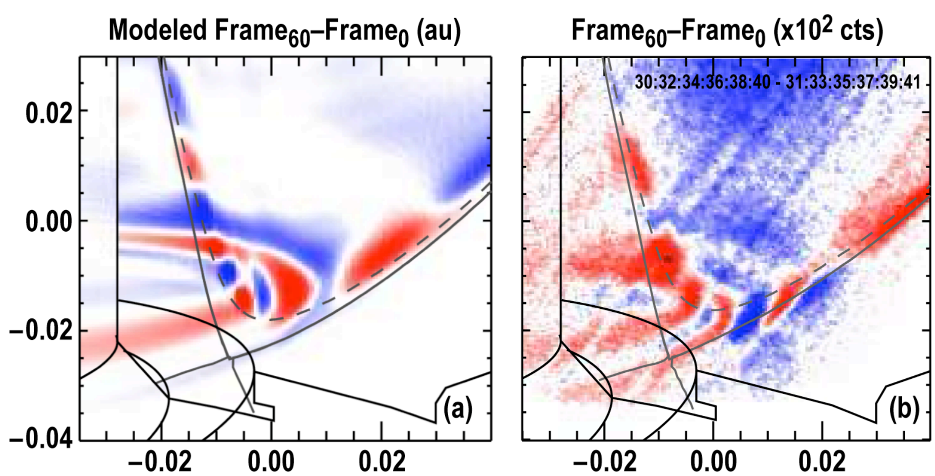

Fig. 4. The modeled (a) and measured (b) differential soft x-ray signal between two opposite phases of the I-coil, for a DIII-D discharge operated in even-parity n=3 configuration.

3.4. DISRUPTION MODELING

Gas-Jet Study: An appreciable resistivity enhancement on the outermost flux surfaces is needed in order to promote a series of “secondary disruptions” in the current quench (CQ) phase, intended to de-confine runaway electrons using the repetitive gas injection scheme of

Putvinski. In addition to modifying the external plasma resistivity by the propagation of outgoing “cooling waves” along the magnetic lines of force intercepting the jet, the interior region of the jet is insulated from the plasma electron heat flux because it is cold and dense. Nevertheless, it is by no means protected from the presence of the plasma because the gas suffers from an electrical discharge breakdown by virtue of the fact that the body of the jet, being a good insulator, initially blocks the (parallel) current pathway, and thus acts like a large-scale circuit breaker to the high-impedance (inductive) tokamak plasma current.

In general gas discharges still suffer from a lack of comprehensive understanding, in part because there is such a variety of different discharge classifications and chemical processes. What we have learned is that the jet discharge plasma in this situation will be dominated by the formation of molecular (dimer) ions formed by the three-body atom assisted process. Since the process is three-body, it means that it will be exceeding fast when the gas is cold and the density is high, as it will be initially for a high Mach number supersonic jet penetrating the plasma. A substantial concentration of dimer ions will dominate the electron annihilation physics, as the dissociative recombination of the molecular ions is orders of magnitude larger than the ordinary rate of atomic ion recombination at typical ~1 eV electron gas discharge temperatures. As a result, the electron concentration will be very small and the gas jet electrical resistance very high. The fractional electron concentration shows a dramatic depression when the electron temperature is below a critical temperature

Another resistivity enhancement mechanism stems from the excitation of current driven ion-acoustic instability. This is possible inside the cold resistive jet, and could lead to a large anomalous resistivity. The current-driven ion acoustic instability can lead to a larger than classical anomalous resistivity by factors of 10 to 100. The instability will shut off when the gas warms up and expands. Hence, the dynamic expansion needs to be treated self consistently with the resistive heating.

NIMROD Poloidally Asymmetric Massive Gas injection Simulations: The impurity injection source term has been modified in NIMROD to allow massive gas injection (MGI) simulations with impurities deposited only on the high-field-side or low-field-side to compare with previous poloidally symmetric MGI simulations. An initial set of DIII-D simulations with neon MGI have been carried through the initial assimilation phase in which neutral impurities deposited mainly in the vacuum region diffuse into the plasma, ionizing as they reach the separatrix. The pre-thermal-quench phase continues until the destabilization of MHD modes initiates the thermal quench (TQ) in each case. A TQ onset time of just over 2 ms is found for both the high-field-side and low-field-side injection, identical to the poloidally symmetric injection results. This simulations must be carried through the end of the TQ phase to assess how the MHD mixing associated with the 1/1 mode differs for the various impurity injection locations.

Radiation Asymmetry and Impurity Mixing in NIMROD MGI Simulations: In a set of NIMROD simulations, massive gas injection in DIII-D has been modeled with varying poloidal and toroidal impurity source distributions. These simulations reveal that even a perfectly toroidally symmetric impurity source produces radiation asymmetry due to the role of the 1/1 mode in convecting both heat from the core to edge and impurities from edge to core. The symmetric case has a radiation toroidal peaking factor (TPF) of about two. With an asymmetric source, the phase of the 1/1 mode is found to determine the location of the radiation toroidal peak, not the injection location of the impurities. The radiation is peaked at the location where the hot core is convected outward toward the impurities at the edge, not where impurities are convected inward. The location of the source sets the 1/1 mode phase in the simulations, since there are no other significant asymmetries in the initial conditions. Comparison of low-field-side with high-field-side injection indicates that variation of the poloidal injection location can qualitatively affect the spectrum of MHD modes that appear. The presence of a dominant n=2 mode rather than n=1 appears to reduce the radiation TPF.

3.5. IDEAL STABILITY MODELING

DIII-D Ideal Stability Analysis: Initial analysis from the 2011 and 2012 Torkil Jensen Award experiments, intended to document a helical core equilibrium embedded in an axisymmetric exterior and to obtain operation in DIII-D with q_{95} below 2.0, suggests both were largely successful. In the former experiment, while a continuous helical core with sawtooth suppression was not observed, possible evidence for the helical core was seen from a continuous oscillation on the ECEI system during extended periods between and across sawtooth periods, and independent of the sawtooth precursor. The latter experiment was successful in producing several candidate diverted discharges with $q_{95} \sim 1.9$.

4. ADVANCES IN TRANSPORT RESEARCH

4.1. GYRO IMPROVEMENTS AND APPLICATIONS

GYRO and TGYRO Developments: GYRO and TGYRO were modified to enable operation in so-called hybrid mode that combines distributed-memory parallelization using MPI with shared-memory parallelization using OpenMP. Initial timing tests are very favorable, showing performance improvements up to the maximum number of OpenMP threads per NUMA node (8 threads per node on Cray XK6 and 6 threads per node on Cray XE6). The user scripts and platform files were also modified to aid the user in setting up and submitting jobs, which is very complex at the system level.

GYRO Simulations with External Magnetic Perturbations: As described previously, our study of GYRO simulations with external resonant magnetic perturbations (RMPs) has been able to compute the island screening response from the island stability parameter Δ. The island phase lag angle and actual width can be calculated from Δ via the inner-outer asymptotic matching formula and the known vacuum island width. Δ depends on the turbulence intensity and the radial electric field providing the plasma $E{\times}B$ rotation. The imaginary part is proportional to the Maxwell stress and controls the island phase angle as it is pushed away from locking to the external field by the plasma $E{\times}B$ rotation. The real part controls the screening that is minimal near the electron rest point in agreement with recent DIII-D analysis of RMP screening by Heyn (2008) and Ferraro (2011).

Nonlinear Theory of Drift-Cyclotron Kinetics and the Breakdown of Gyro-Kinetics: The search for the 5-10 fold missing L-mode edge transport and turbulence has motivated research to test for the breakdown of gyro-kinetics and gyro-averaging at high turbulence levels found at the edge. We have recently formulated a nonlinear theory of drift-cyclotron kinetics that we term *cyclo-kinetics*. Gyro-kinetics extends drift kinetics to micro-turbulence scales on the order of the ion gyro-radius, but is limited to low-drift wave frequencies much less than the cyclotron frequency $\omega \ll \Omega$ and low turbulence levels such that the perturbed $E{\times}B$ motion is less than the ion thermal speed $\delta \upsilon_E \ll \upsilon_{th}^i$. Cyclo-kinetics (CK) is more fundamental, extending 5D gyro-kinetics (GK) to 6D by dynamically including time advance of the gyro-phase (α). Our nonlinear δf formulation is a straight forward transformation of 6D Cartesian coordinates $\left[\vec{x},\vec{\upsilon}\right] \rightarrow [\vec{x}',\mu,\alpha,u]$ where μ is the magnetic moment, u is the parallel velocity, To set up a simple 4D CK $[k_x,k_y,\mu,\alpha]$ problem, we consider electrostatic turbulence in a straight shearless magnetic field $[k_x,k_y,\mu,\alpha]$ to be compared with the corresponding 3D GK $[k_x,k_y,\mu]$ problem.

Assuming nearly adiabatic electrons, the density and ion temperatures combined with a ∇B drift will provide a test model ITG-ai turbulent transport. To work in k-space and avoid non-local profile variation effects, the formulations is limited to low $\rho_* = 1/\Omega_* \sim O(1\%)$ where Ω_* is the normalized cyclotron frequency. The 4D CK system can be simulated on gyro-phase, a 2N+1 α-grid, but comparison with 3D GK is made more transparent by transforming to a basis of $-N < n < N$ cyclotron harmonics, which have linear frequencies near $n\Omega$. Keeping only the 0-th CK harmonic is linearly identical to GK, except we have shown that CK nonlinearity is about half that of GK. This suggests CK transport will be at least twice as large as GK transport (even discounting the additional free energy extracted by unstable cyclotron modes). Of course just keep the first harmonics $n = \pm 1$ requires a time-step 100 times smaller and the nonlinear term becomes very complicated with μ-derivatives. Work is in progress with a PKU graduate student to extend the existing nonlinear 3D GK code to 4D CK and adding the cyclo-kinetics. The linear 4D CK eigen-solver code is straight forward, but the nonlinear simulations will be quite a challenge even for a highly reduced problem.

New Gyro-kinetic Code Development for Highly Collisional Plasmas: Further development of a new gyro-kinetic code for use in micro-instability studies of plasmas in highly collisional regimes was continued. The code solves the linear, multi-species, electrostatic gyro-kinetic equation in the flux-tube limit with a model collision operator (Connor or zeroth-order Hirshman-Sigmar) that includes full cross-species collisional coupling. The algorithm is similar to NEO, using a time-stepping algorithm that is fully implicit to ensure high-accuracy of the collision operator. The code has been benchmarked with GYRO for linear ITG physics and the collisional zonal flow damping, including full mass-ratio gyro-kinetic electrons. While high resolution in θ (the poloidal angle) and pitch angle resolution are expected to be needed at low collisionality due to the discontinuity in the collisionless distribution function across the trapped/passing particle boundary, it is found that even in the highly-collisional limit many grid points in θ are needed to fully resolve the structure of the gyro-kinetic eigenmodes in these coordinates, usually more than twice as many for the equivalent neoclassical simulation.

4.2. GYRO ENERGETIC PARTICLE SIMULATIONS

GYRO Energetic Particle Simulations: An ongoing linear benchmarking and validation effort around DIII-D discharge 142111 was concluded, yielding excellent agreement with experimental spectrograms and eigenmode structure measurements over most of the reverse shear Alfvén eigenmode (RSAE) sweep range. Disagreement between GYRO and experiment at the low end of the sweep, defined by coupling to the beta induced Alfvén eigenmode (BAE), suggests the form of the driving energetic-particle (EP) distribution function plays an important role in determining the real frequency of Alfvén-sonic modes such as the BAE. The correct distribution is also critical for accurately calculating the growth rate for all EP-driven modes. These realities have motivated an investigation into a significant GYRO code development project to generalize the velocity-space dependence of equilibrium distribution functions, long considered prohibitively large in scope. A manageable approach to implementing alternate distributions has been identified, beginning with a non-Maxwellian, isotropic form (e.g., slowing-down). A later extension to anisotropic distributions is also found to be feasible.

Comparison of AE linear flux footprints was facilitated by the adoption of the following simple saturation assumption: $\Gamma_{EP}^{peak} \propto \gamma$. Here, Γ_{EP}^{peak} is the peak density flux of the energetic beam ions and γ is the linear growth rate of the flux-driving mode. Then the saturated value Γ_{nl} of any flux Γ is assumed to obey $\Gamma_{nl} \propto \gamma(\Gamma/\Gamma_{EP}^{peak})$. Under this saturation assumption, the flux prediction of local simulations matches extremely well to the 100 (or more) times more computationally intensive global simulations. A sequence of local simulations captures the globally predicted energetic particle (EP) flux profile extraordinarily well, even when flux is driven by the fundamentally global RSAE (Fig. 5). By selecting the local TAE from each local spectrum rather than the largest flux, the global TAE flux footprint is very accurately recovered, excepting a tail region where no local instabilities exist. This small tail flux may be thought of as a non-local effect. Similar correspondence exists for the thermal ion flux. A series of thermal ion pinches and outward flux driven by the TAE may be of interest for driving zonal flows and possibly mitigating core micro-turbulent stiffness.

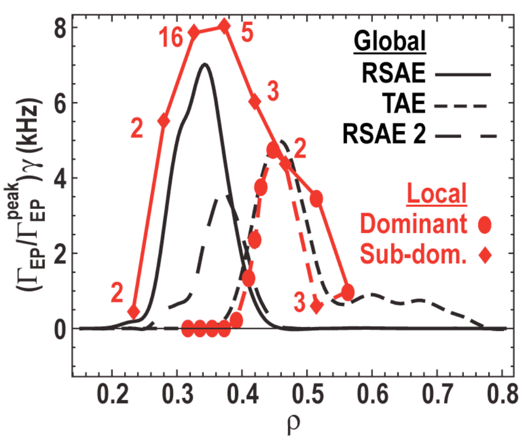

Fig. 5. Comparison of globally predicted energetic-particle (EP) and thermal-ion fluxes against local approximations for DIII-D discharge 142111 with a simplified saturation mode.

Attempts to yield states of global Alfvén eigenmodes saturated by quasi-linear relaxation in GYRO have proved extremely elusive. Removing the long-wavelength source allows global profile relaxation, but perturbations always propagate to the edge and accumulate against the δf=0 boundary condition, leading to runaway. Efforts to remedy the runaway, including resolution adjustment (in time, and velocity space) and changes to the driving EP profile, have failed. Alfvén-like runaway states result even when the equilibrium is linearly stable to Alfvén eigenmodes, suggesting a fundamental numerical problem with the EP species may exist. Even given the GYRO boundary conditions, a saturated state is, in principle, possible for a sufficiently small-scale and weak initial instability.

A simple analytic quasi-linear model of EP transport in radius and energy (r,ε) by micro-turbulence (based on TGLF spectral weights) was developed. The model shows acceptable agreement (with a justifiable scale factor) with GYRO EP transport for the diagonal component of the diffusion tensor giving simple radial diffusion, but fails for the off-diagonal component that gives rise to the effective radial pinch in cases of weak density gradients.

TGLF Quasi-Linear Model for Passive Kinetic Diffusion of Energetic Particles: As part of the GSEP-SciDAC project, a model for passive kinetic diffusion of energetic particles (EP) has been formulated and TGLF driven code DEP has been completed. Here, "passive" means that the turbulence is driven by the ITG/TEM unstable modes and not EP driven Alfvén modes (that likely saturate by relaxation to a critical EP pressure gradient). The EPs are essentially test particles. "Kinetic" means the diffusion is in radial as well as in velocity space. The main application will be to compute the effect of ITG/TEM turbulence on DIII-D off-axis NBI current drive, where the EP distribution is far from Maxwellian. The DEP code was tested against GYRO simulations and a Physics of Plasmas paper is in GA review.

4.3. TGLF TRANSPORT MODEL DEVELOPMENT AND VALIDATION

TGLF Analysis and modeling of DIII-D Experiments: Analysis and TGLF modeling of the recent DIII-D ion stiffness H-mode experiments was continued. TGLF modeling of 26 discharges from these experiments shows that the temperature profile shape varies weakly with the NBI power even though the power has varied over a factor of 3 consistent with experimental observations (Fig. 6). The electrons appear to be stiffer than the ions. A change in the $E\times B$ shear as the NBI power is increased due to difference in the toroidal rotation likely accounts for the ions appearing to be less stiff.

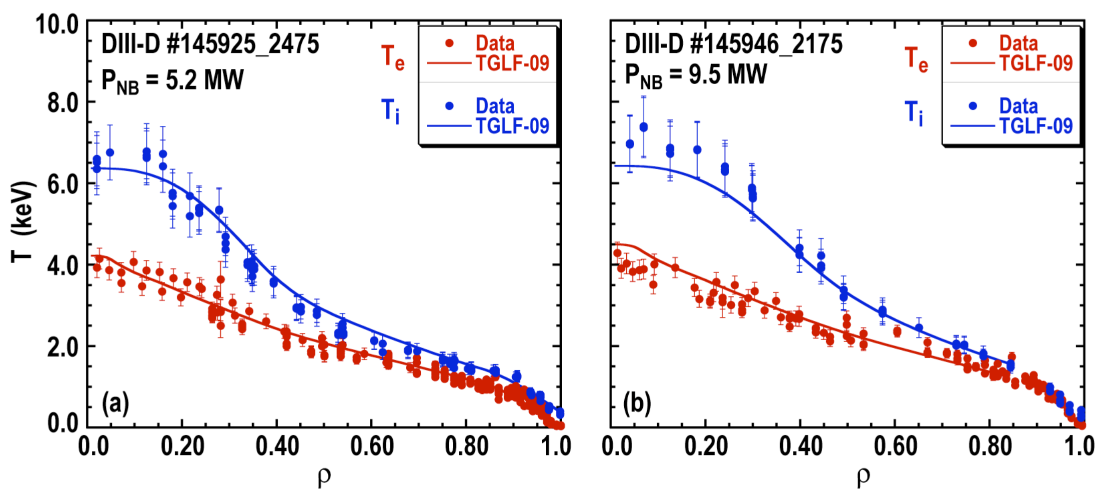

Fig. 6. Comparison of temperature profiles for two H-mode discharges from a DIII-D stiffness experiment with 5.2 MW (a) and 9.5 MW (b) of NBI injection.

TGLF has also recently been used to examine the effect of radially extending the location of the minimum safety factor in reversed-shear low and high beta DIII-D discharges. In the absence of $E\times B$ shear stabilization, which is what is expected in FDF, it is found that the incremental stored energy increases linearly with the location of the minimum safety factor based on modeling results of representative low and high beta DIII-D reversed-shear discharges. Extending the location of the minimum safety factor also broadens the pressure profile that suggests improved MHD stability.

TGLF Momentum Transport Development: The new "spectral-shift" paradigm for $E\times B$ Doppler shear was improved and brought to a final form after extensive verification with GYRO results. The new model does a better job with internal transport barriers but is also numerically more challenging than the quench rule in XPTOR. A new numerical technique was found that greatly helps to stabilize the Newton iterations when momentum transport is evolved. A relaxation/governor is applied to the update of the Doppler shear separately from the parallel velocity shear. This combined with only using the parallel velocity shear variations in computing the Jacobian of derivatives damps unwanted barriers and keeps the Newton direction from getting stuck at fixed points.

TGLF was also modified to use the actual GYRO spectrum of the electric potential fluctuation amplitude without $E\times B$ shear and the spectral shift from the GYRO simulations in a simple quasi-linear model. TGLF was used to calculate the linear eigenmodes at the shifted peak of the spectrum to determine the quasi-linear weights that produce the Reynolds stress and other fluxes. This eliminated any fitting other than the spectral shift model. The results for the fluxes and stress were even better than what was obtained for TGLF with a fit to the wave-number shift and the TGLF model for the saturated electric potential amplitude.

4.4. NEOCLASSICAL TRANSPORT AND FLOW

3D Local Analytic Equilibrium Solver for in Neoclassical Simulations: Toroidal non-axisymmetry effects were considered for implementation in the neoclassical code NEO. For the equilibrium, a new 3D local analytic equilibrium solver, analogous to a 3D extension of the Miller formalism for shaped axisymmetric equilibria, based on the formalism developed by C. Hegna is being developed. This is non-trivial, particularly since a solution to the MHD equilibrium equations is not guaranteed to exist for a given parameterization, but will be essential for systematic studies of the effects of 3D flux-surface shaping parameters and for gaining insight on the 3D effects on neoclassical transport. While reduction of the method to the axisymmetric limit has been successful, development of a generalized numerical method to solve the PDEs in 3D, first focusing on quasi-symmetric configurations, is ongoing.

Effects of Collision Models on Neoclassical Transport in the Plasma Edge: NEO has been used to assess the limitations of commonly used model collision operators for realistic edge-relevant parameters by comparing the neoclassical transport levels predicted by the exact full linearized Fokker-Plank collision operator to those from various model operators in DIII-D L-mode plasmas. Previously for these cases NEO simulations of the deuterium and carbon flows were shown to agree with measurements upon approach to the last closed flux surface. We considered four model collision operators: test particle with an ad hoc field particle operator, full Hirshman-Sigmar, zeroth order Hirshman-Sigmar, and Connor.

For both the high and low density cases, the ad hoc field particle operator and the zeroth order Hirshman-Sigmar are the most accurate for the flows as well as for the bootstrap current, with less than 10% error for the latter and between 20–30% for the flows. The Connor model and the zeroth order Hirshman-Sigmar, which are most closely related in that they contain only the Lorentz operator with a simple momentum-restoring term, underestimate the bootstrap current, while the ad hoc field particle and full Hirshman-Sigmar operators, which both contain energy diffusion terms, generally overestimate the bootstrap current. All of the models underestimate the carbon flow further in the edge. A notably large inaccuracy of the full Hirshman-Sigmar model, especially at higher collision frequency closer to the edge, is surprising, although it has been shown to significantly underestimate the ion flow coefficient for pure plasmas at large collisionality. Overall, the results show that using the full linearized Fokker-Planck operator becomes more important further into the edge.

5. ADVANCES IN RF HEATING AND FUELING RESEARCH

5.1. ORBIT-RF SIMULATIONS

ORBIT-RF Simulations of DIII-D High-Harmonic Fast-Wave Experiments: For quantitative comparison of computed fast-ion distributions with measurements, a series of self-consistent simulations using the 5D finite-orbit Monte-Carlo code ORBIT-RF coupled with the full-wave code AORSA was performed by scanning the assumed fraction of core fast-wave (FW) power absorption. The fast-ion distributions that yield the neutron enhancement factor comparable to the experimental ones are passed to the fast-ion diagnostic simulation code FIDASIM to compute the synthetic fast-ion D_α (FIDA) signals. ORBIT-RF/AORSA reproduces the synergistic effect measured in neutron reaction rates and vertical FIDA signals in the two-frequency FW heating (4th harmonic 60 MHz and 6th harmonic 90 MHz) compared to those obtained in a single-frequency FW heating (4th harmonic 60 MHz). For the tangential FIDA signals, ORBIT-RF/AOSA also reproduces the trend of the measured FIDA signals, which indicate that the tangential components of the fast ions are hardly accelerated by either a single-frequency FW or two-frequency FW. This synergy arises from finite Larmor radius effects that occur since a substantial fraction of fast ions above the neutral-beam injection energy is present due to preheating by the 60 MHz FW. Therefore, the additional 90 MHz FW damps significantly on the beam-ion tails and produces a synergy.

5.2. PELLET ABLATION MODEL

Development of Pellet Ablation Models: A special pellet ablation theory was developed for modeling pellets with essentially "zero" sublimation energy. A general pellet-ablation model was also developed that unifies the ablation dynamics of pellet species of arbitrary atomic number with finite sublimation energy based on a Fokker-Planck treatment of the electron heat-flux attenuation in the expanding ablation shield. The model was applied to predict the penetration depth and density profile in ITER after injection of a Be pellet. The results suggest that deep penetration is possible with modest pellet velocities.

6. ADVANCES IN INTEGRATED MODELING

6.1. IMFIT / OMFIT DEVELOPMENT AND APPLICATIONS

The IMFIT kinetic EFIT GUI was significantly improved to enhance its user friendliness. These include a more flexible multiple time-slice analysis capability and a current density constraint option from ONETWO. The CQL3D Fokker-Planck module was also integrated to run under the IMFIT framework.

A new improved Python-based integrated modeling framework OMFIT was developed that facilitates efficient interactions among modules by treating files, data, and scripts as a collection of objects organized in a MDSPlus-like tree structure. A large number of physics models including kinetic EFIT, GATO, GKS, and TGLF_LS was integrated into OMFIT. Other recent enhancements include a new module to drive the ONETWO/GCNMP transport package, a new neoclassical toroidal viscosity module to compute torque, and a new magnetic-flutter transport module.

A DIII-D transport study using ONETWO/GCNMP was completed. Experimental temperature profiles and energy fluxes for a set of twenty DIII-D discharges with and without an internal transport barrier were analyzed and compared against predictions from the GLF23 transport model. Results from ONETWO/GCNMP show that generally the GLF23 predicted temperature profiles and energy fluxes in discharges without an internal transport barrier agree better with the experimental profiles and fluxes than those with an internal transport barrier.

6.2. ONETWO TRANSPORT CODE DEVELOPMENT

ONETWO Development: A new version of the TGLF turbulent transport module and supporting routines from the GitHub repository was installed into the ONETWO/GCNMP transport package. A parallel communicator was developed to support the new calling method used by this TGLF version. The new interface allows passing of data to communicator groups rather than just individual processors. The NETCDF interface data files were also enhanced to allow for time-dependent RF power from each gyrotron. A new version of the multimode transport model that includes ITG, TEM, ETG, and drift resistive ballooning modes was also implemented into the GCNMP transport module.

7. PUBLICATIONS

PRIMARY THEORY AUTHORS FOR 2012

E.M Bass and R.E. Waltz, "Gyro-Kinetic Study of the unstable Alfvén Eigenmode Spectrum in a Reversed Shear Discharge," submitted to Phys. Plasmas, 2012.

E.A. Belli and J. Candy, "Full Linearized Fokker-Planck Collisions in Neoclassical Transport Simulations," Plasma Phys. Control. Fusion **54**, 015015 (2011).

R.V. Bravenec, J. Candy, M. Barnes, and C. Holland, "Linear and Nonlinear Verification of Gyro-Kinetic Microstability Codes," Phys. Plasmas **18**, 122505 (2011).

N.M. Ferraro, "Symmetries of Resistive Two-Fluid Magnetohydrodynamics under Reversal of Toroidal Field, Current, and Rotation," Phys. Plasmas **19**, 014505 (2012).

N.M. Ferraro, "Calculations of Two-Fluid Linear Response to Non-Axisymmetric Fields in Tokamaks," Phys. Plasmas **19**, 056105 (2012).

W. Guttenfelder, J. Candy, S.M. Kaye, W.M. Nevins, R.E. Bell, G.W. Hammett, B.P. LeBlanc and H. Yuh, "Scaling of Linear Micro-Tearing Stability for a High Collisionality National Spherical Torus Experiment Discharge," Phys. Plasmas **19**, 022506 (2012).

N.T. Howard, M. Greenwald, D.R. Mikkelsen, A.E. White, M.I. Reinke, D. Ernst, Y. Podpaly and J. Candy, "Measurement of Plasma Current Dependent Changes in Impurity Transport and Comparison with Nonlinear Gyro-Kinetic Simulation," Phys. Plasmas **19**, 056110 (2012).

C. Holland, J.C. DeBoo, T.L. Rhodes, L. Schmitz, J.C. Hillesheim, G. Wang, A.E. White, M.E. Austin, E.J. Doyle, W.A. Peebles, C.C. Petty, L. Zeng and J. Candy, "Testing Gyrokinetic Simulations of Electron Turbulence," Nucl. Fusion **52**, 063028 (2012).

C. Holland, C.C. Petty, L. Schmitz, K.H. Burrell, G.R. McKee, T.L. Rhodes and J. Candy, "Progress in GYRO Validation Studies of DIII-D H-Mode Plasmas," Nucl. Fusion **52**, 114007 (2012).

N.T. Howard, M. Greenwald, D.R. Mikkelsen, M.L. Reinke, A.E. White, D. Ernst, Y. Podpaly, and J. Candy, "Quantitative Comparison of Experimental Impurity Transport with Nonlinear Gyrokinetic Simulation in an Alcator C-Mod L-mode Plasma," Nucl. Fusion **52**, 063002 (2012).

V.A. Izzo, E.M. Hollmann, A.N. James, J.H. Yu, D.A. Humphrey, L.L. Lao, P.B. Parks, P.E. Sieck, J.C. Wesley, R.S. Granetz, G.M. Olynyz, and D.G. Whyte, "Runaway Electron Confinement Modeling for Rapid Shutdown Scenarios in DIII-D, Alcator C-Mod and ITER," Nucl. Fusion **51**, 063032 (2011).

V.A. Izzo, D.A. Humphrey, and M. Kornbluth, "Analysis of Shot-to-Shot Variability in Post-Disruption Runaway Electron Currents for Diverted DIII-D Discharges," Plasma Phys. Control. Fusion **54**, 095002 (2012).

J.E. Kinsey, G.M. Staebler, R.E. Waltz, and R.V. Budny, "ITER Predictions Using the GYRO Verified and Experimentally Validated Trapped Gyro-Landau Fluid Transport Model," Nucl. Fusion **51**, 083001 (2011).

P.B. Snyder, T.H. Osborne, K.H. Burrell, R.J. Groebner, A.W. Leonard, R. Nazikian, D.M. Orlov, O. Schmitz, M.R. Wade, and H.R. Wilson, "The EPED Pedestal Model and ELM-Suppressed Regimes: Studies of Quiescent H-Mode and Development of a Model for ELM Suppression via Resonant Magnetic Perturbations," Phys. Plasmas **19**, 056115 (2012).

D.A. Spong, E.M. Bass, W. Deng, W. Heidbrink, Z. Lin, B. Tobias, M. Van Zeeland, M.E. Austin, C. W. Domier, N. C. Luhmann, Jr., "Verification and Validation of Gyrokinetic Simulation of Alfvén Eigenmodes in the DIII-D Tokamak," Phys. Plasmas **19**, 082511 (2012).

G.M. Staebler, J.E. Kinsey, and R.E. Waltz, "A New Paradigm for Suppression of Gyro-Kinetic Turbulence by Velocity Shear," submitted to Phys. Rev. Lett., 2012.

B.J. Tobias, E.M. Bass, I.G.J. Classen, C.W. Domier, B.A. Grierson, W.W. Heidbrink, N.C. Luhmann, Jr., R. Nazikian, H.K. Park, D.A. Spong, and M.A. Van Zeeland, "Alfvén Eigenmode Structure during Off-Axis Neutral Beam Injection," Nucl. Fusion **52**, 103009 (2012).

A.D. Turnbull, W.A. Cooper, L.L. Lao and Long-Poe Ku, "Ideal MHD Spectrum Calculations for the ARIES-CS Configuration," Nucl. Fusion **51**, 123011 (2011).

A.D. Turnbull, "Plasma Response Models for Non-Axisymmetric Perturbations," Nucl. Fusion **52**, 054016 (2012).

R.E. Waltz and Zhao Deng, "Nonlinear Theory of Drift-Cyclotron Kinetics and the Breakdown of Gyro-kinetics," submitted to Phys. Plasmas, 2012.

R.E. Waltz and F.L. Waelbroeck, "Gyro-Kinetic Simulations with External Resonant Magnetic Field Perturbations: Island Torque and Non-Ambipolar Transport with Plasma Rotation," Phys. Plasmas **19**, 032508 (2012).

E. Wang, X. Xu, J. Candy, R.J. Groebner, P.B. Snyder, Y. Chen, S.E. Parker, W. Wan, G. Lu, and J.Q. Dong, "Quantitative Comparison of Experimental Impurity Transport with Nonlinear Gyrokinetic Simulation in an Alcator C-Mod L-mode Plasma," Nucl. Fusion **52**, 103015 (2012).

ACKNOWLEDGMENT

This work supported by the U.S. Department of Energy under Grant No. DE-FG02-95ER54309.